Vat Sun; Attakorn Asanakham; Thoranis Deethayat; Tanongkiat Kiatsiriroat

Article

A new method for evaluating nominal operating cell temperature (NOCT) of unglazed photovoltaic thermal module

Energy Reports

Provided in Cooperation with:
Elsevier

Suggested Citation: Vat Sun; Attakorn Asanakham; Thoranis Deethayat; Tanongkiat Kiatsiriroat (2020) : A new method for evaluating nominal operating cell temperature (NOCT) of unglazed photovoltaic thermal module, Energy Reports, ISSN 2352-4847, Elsevier, Amsterdam, Vol. 6, pp. 1029-1042,
https://doi.org/10.1016/j.egyr.2020.04.026

This Version is available at:
https://hdl.handle.net/10419/244098

Energy Reports 6 (2020) 1029–1042

Contents lists available at ScienceDirect

Energy Reports

journal homepage: www.elsevier.com/locate/egyr

Research paper

A new method for evaluating nominal operating cell temperature (NOCT) of unglazed photovoltaic thermal module

Vat Sun [a], Attakorn Asanakham [b,c], Thoranis Deethayat [b,c], Tanongkiat Kiatsiriroat [b,c,*]

[a] Energy Engineering Program, Department of Mechanical Engineering, Faculty of Engineering and Graduate School, Chiang Mai University, 239 Huay Kaew Road, Muang District, Chiang Mai, 50200, Thailand
[b] Department of Mechanical Engineering, Faculty of Engineering, Chiang Mai University, 239 Huay Kaew Road, Muang District, Chiang Mai, 50200, Thailand
[c] Research Center for Renewable Energy, Faculty of Engineering, Chiang Mai University, 239 Huay Kaew Road, Muang District, Chiang Mai, 50200, Thailand

ARTICLE INFO

Article history:
Received 8 January 2020
Accepted 15 April 2020
Available online xxxx

Keywords:
Photovoltaic thermal module
Nominal operating cell temperature
Module temperature
Performance

ABSTRACT

Photovoltaic thermal (PVT) modules convert solar energy into electricity and heat. Unlike that of normal photovoltaic modules, the nominal operating cell temperature (NOCT) of PVT modules, which is used to evaluate the temperature and electrical power output, is unknown because it depends on the mass flow rate and inlet temperature of the working fluid in the module. In this paper, a new method for calculating the NOCT of PVT modules with water as the working fluid is presented. Four unglazed identical PVT modules in series were tested outdoors with various mass flow rates. The tests, which were similar to solar collector tests, were conducted from 8:30 to 16:30 on clear-sky days in Chiang Mai, Thailand, and the water inlet temperature of the first PVT module of the system was varied from 27 to 60 °C. The correlation between the NOCT of the unglazed PVT module, based on $(T_{fi} - T_a)/I_T$, and the water mass flow rate, $\dot{m}$, was determined. The calculated PVT module temperature determined with the new NOCT method agrees well with the experimental data, and 96% of the calculated results deviate only by up to ±10% from the experimental data.

1. Introduction

The increasing world economy causes many concerns regarding energy demand and environmental pollution. The consumption of limited fossil fuels such as coal and natural gas, which are the primary energy resources today, emits greenhouse gases and other emissions. Photovoltaic (PV) technology is one of the most capable and fastest growing renewable energy approaches and will play an essential role in the near future.

Electrical power generated by PV modules depends on many factors: solar irradiance, solar spectrum, PV module installation, and PV module performance. According to manufacturers, the efficiency can be determined under standard test conditions (solar irradiance of 1,000 W/m^2, air mass of 1.5, and operating module temperature of 25 °C). However, in practice, solar irradiance varies with the sun path and cloud condition. When the PV module is exposed to sun irradiance, the operating temperature of the PV module can reach 70 °C, particularly in hot countries such as Thailand in which the ambient temperature sometimes exceeds 40 °C. Consequently, the PV efficiency is lower than that under standard conditions. Fig. 1 shows the PV module performance of different cells at different module temperatures. An increasing PV module temperature decreases the open-circuit voltage and increases slightly the short-circuit current, which results in lower maximum generated power (rectangular area of I–V curve in Fig. 1). Many methods for reducing the solar cell module temperature have been reported: for instance, air, water (Teo et al., 2012), and phase change material (PCM) cooling (Sun et al., 2018).

The active heat removal at the back of a PV module by liquid/air is realized with a PV thermal (PVT) module. In the PVT module, the solar module is attached to an absorber plate with circulating fluid inside for the simultaneous generation of power and hot water or air; the overall module efficiency can be higher than that of the normal PV module. The first design of PVT modules was presented by Kern and Russell in 1978 (Kern and Russell, 1978). In 1979, Florschuetz (1979) developed a theoretical model with experimental studies for the PVT module performance with a solar collector model. Fudholi et al. (2014) studied three different water flow channels for a PVT module: web flow, direct flow, and spiral flow. The spiral flow led to the best PVT module performance. Moreover, Al-Shamani et al. (2016) tested PVT

* Corresponding author at: Department of Mechanical Engineering, Faculty of Engineering, Chiang Mai University, 239 Huay Kaew Road, Muang District, Chiang Mai, 50200, Thailand.
E-mail address: tanongkiat_k@yahoo.com (T. Kiatsiriroat).

https://doi.org/10.1016/j.egyr.2020.04.026

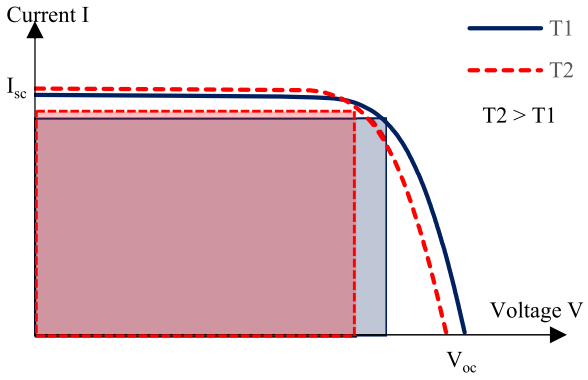

Fig. 1. PV performance at different module temperatures.

modules with various types of nanofluids (SiO_2, TiO_2, and SiC); the results showed that the fluid with SiC resulted in the best performance. Yu et al. (2019) designed an unglazed PVT in which the absorber plate was attached with the thermo-laminating bonding method. As a result, both the electrical and thermal efficiencies were improved. Some PVT modules with PCMs were numerically (Gaur et al., 2017; Fayaz et al., 2019; AL-Musawi et al., 2019; Kazemian et al., 2019) and experimentally (Hossain et al., 2019) studied; their electrical system efficiency was improved from 7.1% to 13%, and the thermal efficiency was 72% (Al-Waeli et al., 2019; Salem et al., 2019). Furthermore, a PVT module was used for combined cooling, heating, and power generation in a building (Ramos et al., 2017; Herrando et al., 2019); the PVT module output covered 60% of the heating demand and 100% of the cooling electricity.

In general, the maximum power generated by the PV or PVT module can be evaluated when the incident solar irradiance and module temperature are known. To determine the module temperature, several mathematical models (dynamic and steady-state) have been developed (Al Tarabsheh et al., 2016; Fiorentini et al., 2015; Rejeb et al., 2015; Shyam and Tiwari, 2016; Guarracino et al., 2019; Al-Shamani et al., 2018). For instance, Rejeb et al. (2015) developed a thermal model of a PVT module with energy balance equations for six main components: transparent cover, PV module, plate absorber, tube, water-filled tube, and insulation. In addition, the energy balance equations included the thermal properties of the PV module and related heat transfer coefficients. Al-Shamani et al. (2018) used the computational fluid dynamics technique to calculate the temperature of a PVT module with water-based nanofluid for heat extraction. Table 1 shows the current models that are used to calculate the PVT module temperature. However, the calculation process remains complicated because much information on the heat transfer characteristics and thermal properties is required. Therefore, the calculation is time-consuming and the approach impractical.

Another method for calculating the PV module temperature is determining the nominal operating cell temperature (NOCT), which was introduced by Ross (1980) in 1980. The NOCT is the module temperature at solar irradiance of 800 W/m^2 and 20 °C. In the method, the module is subjected to various solar irradiance and ambient temperature values to predict the PV module temperature based on a correlation. Normally, the manufacturer provides the NOCT values, and the PV module temperature can be estimated. The correlation results reported by Ross agree very well with the experimental data (Mattei et al., 2006). This method is very efficient and more practical than the other methods in Table 1. The NOCT of a PV module is always constant. However, that of a PVT module depends on the mass flow rate and inlet temperature of the working fluid inside the PVT module. A practical method for evaluating the NOCT of PVT modules has not been presented so far.

In this paper, a novel method for evaluating the NOCT of PVT modules with water circulation is presented. The aim is modifying the concept of the flat plate solar collector with liquid heating to determine the thermal characteristics such as the optical efficiency and heat loss coefficient of the PVT module at different liquid mass flow rates and liquid inlet temperatures. These values are integrated into the NOCT equation to determine the NOCT. The determined NOCT at any liquid mass flow rate and inlet liquid temperature can be used to evaluate the PVT module temperature and generated electrical power. This new concept enables the design and sizing of the PVT modules.

2. Theory

The electrical power generation of PV modules depends on the module temperature and solar irradiance. The maximum electrical power can be calculated as follows (Pantic et al., 2016):

$$P_m = P_{m,stc} \cdot (1 - \gamma\,(T_{PV} - 25)) \cdot \frac{I_T}{1000}, \tag{1}$$

where P_m is the maximum electrical output power and $P_{m,stc}$ the maximum electrical power under the standard test conditions at solar irradiance of 1000 W/m^2 and PVT module temperature of 25 °C; γ is the temperature coefficient of the maximum power and T_{PV} the PV module temperature (Ross, 1980; Masters, 2004; Duffie and Beckman, 2013):

$$T_{PV} = T_a + (NOCT - 20) \cdot \frac{I_T}{800}. \tag{2}$$

The NOCT is determined by the PV cell or module temperature, which can be determined with a typical installation at a solar irradiance level of 800 W/m^2, ambient temperature of 20 °C, and under no-load condition. The NOCT is generally provided by the manufacturer and is approximately 45 ± 2 °C for monocrystalline and polycrystalline PVs.

2.1. NOCT and module temperature of PV module

This section describes the derivation of Eq. (2). The temperature of a PV module is determined by the energy balance. In an open circuit, the solar energy absorbed by the PV module, $\dot{Q}_s = (\tau\alpha) \cdot I_T \cdot A$, is converted into heat loss, $\dot{Q}_{Loss} = U_L \cdot A \cdot (T_{PV} - T_a)$. The thermal energy balance for the PV module is as follows:

$$(\tau\alpha) \cdot I_T \cdot A = U_L \cdot (T_{PV} - T_a) \cdot A \tag{3}$$

or

$$(\tau\alpha) = \frac{U_L \cdot (T_{PV} - T_a)}{I_T}, \tag{4}$$

where $(\tau\alpha)$ is the optical efficiency of the PV, U_L is the overall heat loss coefficient, and A is the PV module area. At the reference point of the NOCT conditions provided by the manufacturer: $T_{PV} = NOCT$, $T_a = 20$°C, and $I_T = 800$ W/m^2:

$$(\tau\alpha) = \frac{U_{L,noct}\,(NOCT - 20)}{800}. \tag{5}$$

Based on Eqs. (3) and (4), the PV module temperature at any ambient temperature can be calculated as follows:

$$(\tau\alpha) = \frac{U_L(T_{PV} - T_a)}{I_T} = \frac{U_{L,noct}(NOCT - 20)}{800}. \tag{6}$$

Consequently,

$$T_{PV} = T_a + (NOCT - 20)\,\frac{I_T}{800} \cdot \frac{U_{L,noct}}{U_L}. \tag{7}$$

Table 1
Mathematical models for calculating PVT module temperature.

Mathematical model	Details	Type	Ref.
$T_{PV} = T_a + (NOCT - 20) \cdot \frac{I_T}{800}$	General model for predicting module temperature (PV only); T_a is ambient temperature, I_T is solar irradiation, and $NOCT = 45 \pm 2$ °C.	Steady state	Ross (1980), Masters (2004) and Duffie and Beckman (2013)
$(\rho\delta c_p)_{PV} \frac{dT_{PV}}{dt} = \alpha_{PV}\tau_g I_T + (h_r + h_c)_{PV\to g}(T_g - T_{PV}) - P_e + h_{c,PV\to ab}(T_{ab} - T_{PV}) + (k\delta)_{PV}\left(\frac{\partial^2 T_{PV}(x,y)}{\partial x^2} + \frac{\partial^2 T_{PV}(x,y)}{\partial y^2}\right)$	δ_{PV} is thickness of PV panel, T_g is glass temperature, T_{ab} is absorber plate, k_{PV} is thermal conductivity.	Dynamic	Rejeb et al. (2015)
$T_{PV} = T_a + (219 + 832K_t)\frac{NOCT - 20}{800}$	$NOCT = 45$ °C, K_t is hourly clearness index.	Steady state	Conti et al. (2019)
$(mc_p)_{PV} \frac{dT_{PV}}{dt} = \dot{Q}_{cd,PV} - \dot{Q}_{r,g-PV} + \dot{Q}_{c,g-PV} + \dot{Q}_{PV-AB} - \dot{Q}_{PV-A} - P_e$	$\dot{Q}_{cd,PV}$ is heat transfer in solar cell between two adjacent nodes due to conduction, $\dot{Q}_{r,g-PV}$ is heat addition to glass cover of solar cell due to radiation, $\dot{Q}_{c,g-PV}$ is heat addition to glass cover of solar cell due to convection, $\dot{Q}_{PV-AB}$ is fraction of incident irradiance absorbed by solar cell, $\dot{Q}_{PV-A}$ is heat addition to absorber of solar cell due to conduction.	Dynamic	Guarracino et al. (2019) and Guarracino et al. (2016)
$(\rho Vc_p)_{PV} \frac{dT_{PV,i}}{dt} = (1-\eta_{PV})(\tau\alpha)A_i I_T - h_{ci1}A_i(T_{PV,i} - T_{f,i}) - h_c A_i(T_{PV,i} - T_a) - \xi_1\sigma A_i(T_{PV,i}^4 - T_{P,i}^4) - \varepsilon_{PV}\sigma A_i(T_{PV,i}^4 - T_a^4) - \frac{k_{PV}}{z}e_{PV}w(T_{PV,i} - T_{PV,i+1}) - \frac{k_{PV}}{z}e_{PV}w(T_{PV,i} - T_{PV,i-1})$	η_{PV} is PVT electrical efficiency, T_f is fluid temperature, i is node number, σ is Boltzmann constant, k_{PV} is thermal conductivity, w is width of PVT system, e_{PV} is thickness of PV panel, z is length of each region of PVT system.	Dynamic	Liu et al. (2018)
$(Mc_p)_{abs} \frac{dT_{PV}}{dt} = A \cdot I_T - \dot{Q}_u - \dot{Q}_l - P_e$	$(Mc_p)_{abs}$ is absorbed sensible heat capacity, t is time, $\dot{Q}_u$ is useful heat, $\dot{Q}_l$ is heat loss, and P_e is electrical power.	Dynamic	Sakellariou and Axaopoulos (2018)
$T_{PV} = T_{fi} + \frac{\dot{Q}_u}{A \cdot F_R \cdot U_L}(1 - F_R)$	$\dot{Q}_u$ is useful heat rate.	Steady state	Sakellariou and Axaopoulos (2018)
$T_{PV} = T_m + \frac{\dot{Q}_u}{U_{AbsFluid}}$	$U_{AbsFluid}$ is the internal heat transfer coefficient.	Steady state	Lämmle et al. (2017)
$T_{PV} = \frac{(\alpha_c\tau_g\beta_c - \tau_g\beta_c\beta_0 - \tau_g\beta_c\beta_0\eta_0 T_0)I_T + U_{tc,a}T_a + h_{bcr}T_r}{U_{tc,a} + U_{bc,r} - \tau_g\beta_c\beta_0\eta_0 I_T}$	α_c is absorptivity of solar cell, τ_g is transmissivity of glass, β_c is packing factor of solar cell, β_0 is temperature-dependent efficiency factor, η_0 is efficiency under standard conditions, T_0 is cell temperature for optimal cell efficiency, $U_{tc,a}$ is overall heat transfer coefficient from solar cell to ambient, $U_{bc,r}$ is heat transfer from bottom of module to drying chamber, T_r is room temperature.	Steady state	Sahota and Tiwari (2017)
$T_{PV}^{t+\Delta t} = T_{PV}^t + \frac{\Delta t}{(\rho Vc_p)_{Si}}(\alpha I_T - \dot{Q}_{c,T} - \dot{Q}_{c,B} - \dot{Q}_{r,T} - \dot{Q}_{r,B} - P_e)^t$	t is time, Δt is time step, $\dot{Q}_{c,T}$ is energy transferred by convection at top, $\dot{Q}_{cB}$ is energy transferred by convection at bottom, $\dot{Q}_{r,T}$ is energy transferred by irradiance at top, $\dot{Q}_{r,B}$ is energy transferred by irradiance at bottom, P_e is electrical power.	Dynamic	Al Tarabsheh et al. (2016)
$T_{PV} = \frac{(\tau\alpha)I_T + U_{tc,a}T_a + h_{c,p}T_p}{U_{tc,a} + h_{c,p}}$	$U_{tc,a}$ is overall heat transfer coefficient from solar cell to ambient, $h_{c,p}$ is overall heat transfer coefficient from solar cell to blackened absorber plate.	Steady state	Tiwari et al. (2011) and Atheaya et al. (2016)
$T_{PV} = 30 + 0.0175(I_T * CR - 300) + 1.14(T_a - 25)$ $T_{PV,eff} = T_{PV} + (T_{PVT} - T_a)$	CR is concentration ratio, $T_{PV,eff}$ is effective module temperature obtained from experimental data.	Steady state	Tripanagnostopoulos et al. (2005)

In general, $U_L = U_{L,noct}$, which leads to Eq. (2). However, this equation is no longer used when the PV module is installed in a confined space such as a rooftop or building integration. The installed NOCT (INOCT) at the NOCT was estimated by Fuentes (Fuentes, 1987). According to his results, INOCT is −1 to 11 °C higher than the NOCT temperature when the PV is installed on the roof. Furthermore, Eq. (2) cannot be applied for PVT modules that have an absorber plate with circulating fluid and insulation. A method for evaluating the NOCT of PVT modules is presented in the following section.

Table 2
PVT specification (Anon, 2019a).

Cell type	Mono-crystalline
Dimensions	828 mm × 1601 mm × 90 mm
Aperture area	1.326 m^2
Weight	24.4 kg
Number of cells	72
Cell dimensions	125 mm ×125 mm
Maximum power, P_m	200 Wp
Maximum power voltage, V_{mp}	36.5 V
Maximum power current, I_{mp}	5.2 A
Open-circuit voltage, V_{oc}	45.26 V
Short-circuit current, I_{sc}	5.66 A
Electrical efficiency of module, η_{stc}	15.08%
Temperature coefficients of P_m, γ	−0.45%/°C

2.2. NOCT of PVT module

The temperature of a PVT module is determined by the energy balance. Under no electrical load, the solar energy absorbed by the PV module, $\dot{Q}_s = (\tau\alpha) \cdot I_T \cdot A$, is converted into useful energy in the circulating fluid, $\dot{Q}_u = \eta_{th} \cdot I_T \cdot A = \left(\dot{m}c_p\right)_f (T_{fo} - T_{fi})$ and heat loss, $\dot{Q}_{Loss} = U_L \cdot A \cdot (T_{PV} - T_a)$; η_{th} is the useful thermal efficiency, $\left(\dot{m}c_p\right)_f$ the heat capacity rate of the flow fluid, T_{fi} the inlet temperature before entering the PVT module, and T_{fo} the outlet temperature of the PVT module. Thus, the thermal energy balance for the PVT module can be expressed as follows:

$$(\tau\alpha) \cdot I_T \cdot A = \eta_{th} \cdot I_T \cdot A + U_L \cdot A(T_{PV} - T_a), \tag{8}$$

or

$$\eta_{th} = (\tau\alpha) - U_L \frac{T_{PV} - T_a}{I_T}. \tag{9}$$

Such as for the solar thermal collector, the inlet temperature T_{fi} is used for calculating the thermal efficiency:

$$\eta_{th} = F_R\,(\tau\alpha) - (F_R U_L)\,\frac{T_{fi} - T_a}{I_T}, \tag{10}$$

where F_R is the module heat removal factor. Based on Eqs. (9) and (10),

$F_R\,(\tau\alpha) - F_R U_L \frac{T_{fi} - T_a}{I_T} = (\tau\alpha) - U_L \frac{T_{PV} - T_a}{I_T}$.

This leads to the following expression:

$$\frac{T_{PV} - T_a}{I_T} = F_R \cdot \frac{T_{fi} - T_a}{I_T} + \frac{(\tau\alpha)}{U_L} \cdot (1 - F_R)\,. \tag{11}$$

According to Eq. (2), $\frac{T_{pv} - T_a}{I_T} = \frac{NOCT - 20}{800}$, which leads to the following equation:

$$\frac{NOCT - 20}{800} = F_R \cdot \frac{T_{fi} - T_a}{I_T} + \frac{(\tau\alpha)}{U_L} \cdot (1 - F_R)\,, \tag{12}$$

or

$$NOCT = 800 F_R \cdot \frac{T_{fi} - T_a}{I_T} + \frac{(\tau\alpha)}{U_L} \cdot (1 - F_R)\,800 + 20. \tag{13}$$

The module optical efficiency $(\tau\alpha)$ is constant and depends on the PVT absorber material; F_R and U_L alter the mass flow rate of the circulating fluid. Therefore, the NOCT of the PVT module changes with the mass flow rate $(\dot{m})$ and inlet temperature of the working fluid (T_{fi}).

The NOCT and $(T_{fi} - T_a)/I_T$ exhibit a linear relationship, as shown in Fig. 2(a). The slope of the graph is $800F_R$, and the intercept on the NOCT axis is $\frac{(\tau\alpha)}{U_L} \cdot (1 - F_R)800 + 20$; $(\tau\alpha)$ and U_L can be determined based on the correlation between the PVT thermal efficiency (η_{th}) and $(T_{PV} - T_a)/I_T$, as shown in Fig. 2(b).

3. Experimental setup

A set of four identical unglazed 200 Wp PVT modules was installed in series on a roof, as shown in Fig. 3. The PVT modules were facing south with 18° inclination angle toward the latitude of Chiang Mai. The PVT module information is provided in Table 2. The tests were performed outdoors at the Chiang Mai University, Chiang Mai, Thailand.

The experimental equipment consisted of a closed-loop system (Fig. 4), and the PVT set was connected to a 220 L water storage tank with water circulation based on a water pump. A flow meter was installed to measure the water flow rate leaving the pump, and a ball valve was used to adjust the flow rate. A set of K-type thermocouples were installed at the inlet, outlet, and surface of each PVT module, and the temperature values were recorded by an 8-channel data-logger S220-T8. In addition, an MS-602 pyranometer (Anon, 2019c) aligned with the inclined plane of the PVT module was connected to a Hukseflux LI19 (Anon, 2019b) data logger to measure the solar radiation intensity on the PVT plane. The accuracy of each instrument in this test is listed in Table 3, and the uncertainties of the data reduction are provided in Table 4 and Appendix A.1.

The NOCT test was performed in the open-circuit mode; this means that the PVTs were not connected to an external load, as shown in Fig. 4. Under this condition, the first PVT module (PVT1) was connected to a solar analyzer Prova 210 with a maximum current of 12 A. The solar analyzer scanned the operating current of the PVT module from zero to the short-circuit current; it took approximately 25 s to determine the I–V curve. The solar analyzer started working every 5 min.

The experiments were conducted between 8:30 to 16:45 at daytime on clear-sky days with mass flow rates of 1, 2.4, 4, and 6 LPM (liter per minute).

4. Results

4.1. PVT module performance

Fig. 5 presents the water inlet, water outlet, and module temperature profiles of the four PVT modules in series. The experiment was conducted from 8:30 to 16:45 on a clear-sky day in Chiang Mai. The water outlet temperature of the PVT modules increased from the first to the last modules, and the last module reached a maximum temperature of 63.3 °C at 15:00, which decreased slightly with decreasing solar irradiance. In addition, the PVT module temperature increased with increasing solar

Table 3
Sensors and accuracies.

Sensor	Characteristics and measured range	Accuracy
K-type thermocouple	Measures PV module temperature, inlet/outlet temperature, and ambient temperature Range: −270 to 1260 °C	±0.5 °C
Pyranometer MS-602 with data logger Hukseflux LI19	Measures solar irradiation. Range: 0–2000 W/m^2	±1.5%
Solar analyzer Prova 210	0–60 V 0.01–12 A	±1% ±1%

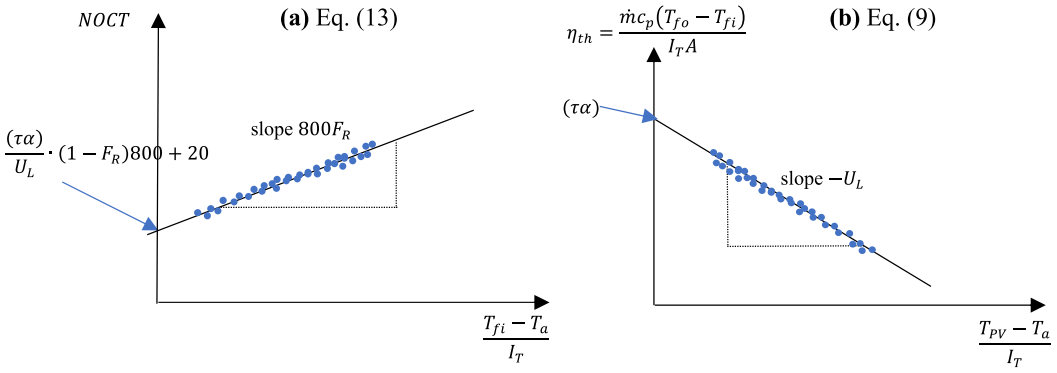

Fig. 2. Relationships between $NOCT$ and $(T_{fi}-T_a)/I_T$ and thermal efficiency η_{th} and $(T_{PV}-T_a)/I_T$. $NOCT=20+800(T_{PV}-T_a)/I_T$ [Eq. (2)].

Fig. 3. (a): Tested unglazed PVT modules and (b) back of module without insulation.

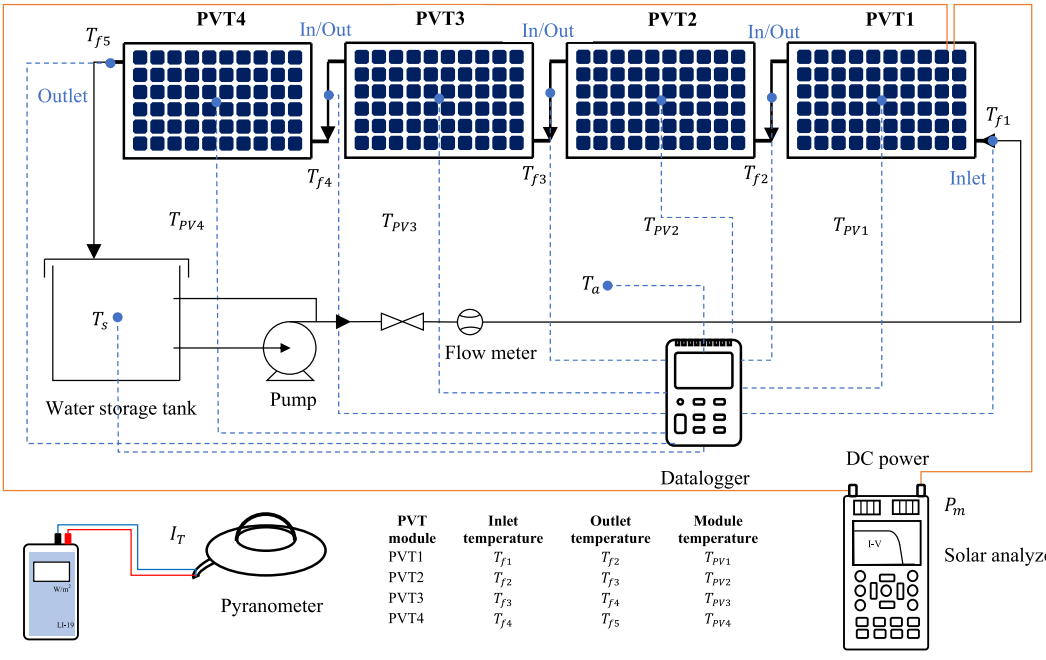

Fig. 4. PVT module performance tests in open-circuit mode.

Table 4
Measurement errors and uncertainties of important parameters.

$\delta T_{a,exp}$	$\delta T_{PV,exp}$	$\delta I_{T,exp}$	$\delta I_{m,exp}$	$\delta V_{m,exp}$	$\delta P_{m,exp}$	$\delta NOCT_{exp}$	$\delta T_{PV,sim}$ (Eq. (2))	$\delta P_{m,sim}$ (Eq. (1))
0.5 °C	0.5 °C	1.5%	1%	1%	1.41%	2.05%	3.45%	1.76%

irradiance and inlet water temperature. At the end of the tests, the PVT module temperatures were higher than those at the beginning because of the higher ambient temperature in the afternoon and the higher temperature in the water storage tank.

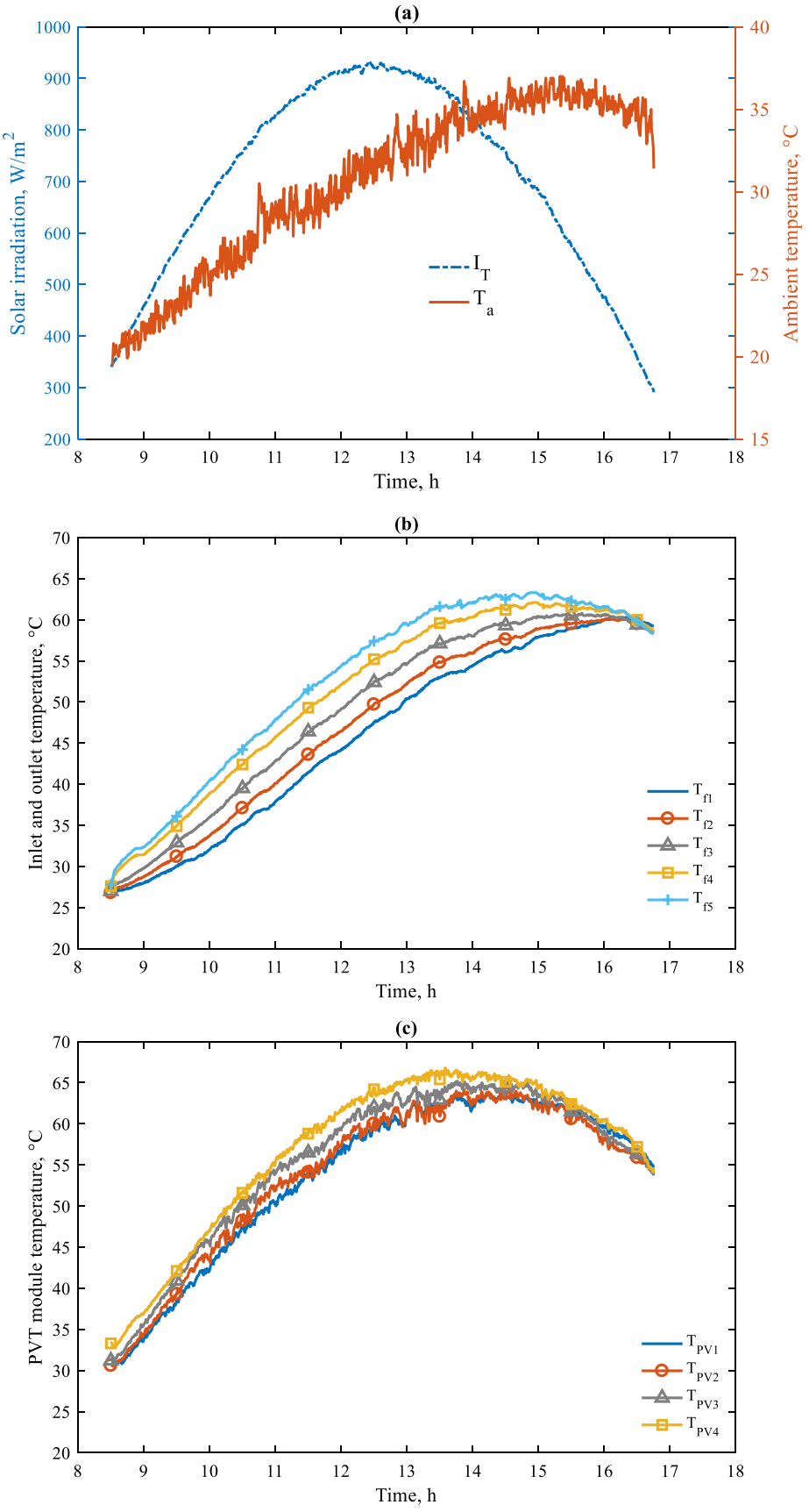

Fig. 5. (a) Weather data, (b) water inlet and outlet temperatures of PVT modules in series, (c) PVT module temperatures on February 10, 2019; water mass flow rate was 2.4 LPM.

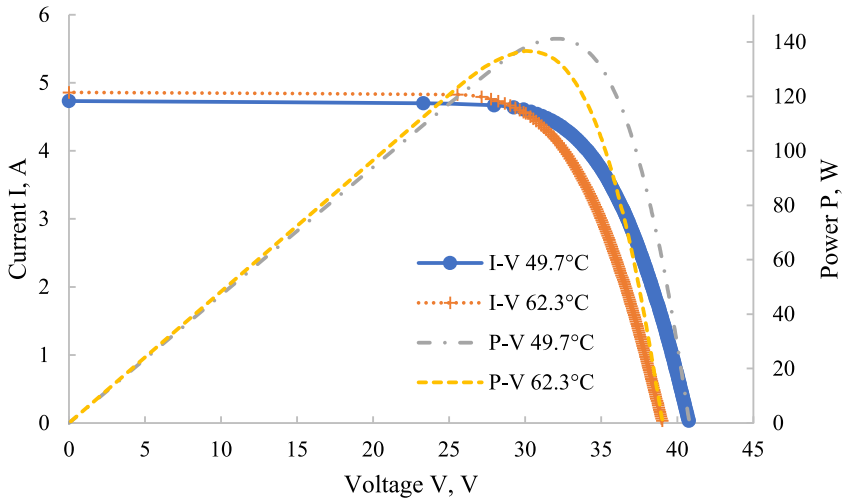

Fig. 6. PVT electrical performance at a solar irradiance of 815 W/m^2 with different module temperatures (results obtained with solar analyzer); tests were performed on February 10, 2019.

The test results of the electrical performance at solar irradiance of 815 W/m^2 is shown in Fig. 6 in forms of I–V and P–V curves. The current in the short-circuit mode increased slightly, and the open-circuit voltage decreased sharply when the PVT module temperature increased. In addition, the maximum power point decreased from 141 to 136 W with increasing module temperature from 49.7 to 62.3 °C.

4.2. NOCT of unglazed PVT module

Fig. 7 shows the PVT thermal performance based on Eqs. (9) and (13). The *NOCT* with respect to $(T_{fi} - T_a)/I_T$ is linear. The optical efficiency of the PVT module, $(\tau\alpha)$, and overall heat loss coefficient, U_L, were calculated based on Fig. 7(b), and the heat removal factor, F_R, was determined with Fig. 7(a).

Based on Eq. (9), the experimental data of the thermal efficiency, η_{th}, with respect to $(T_{PV} - T_a)/I_T$ were plotted in Fig. 7(b). The slope of the plotted curve shows the overall heat loss coefficient, $-U_L$, and the intercept on the thermal efficiency axis is the optical efficiency, $(\tau\alpha)$, of the module.

Since the module temperature was normally over the ambient temperature and $(T_{PV} - T_a)/I_T$ was always higher than 0.02, then there is a lack of datapoints at zero-loss condition. Therefore, there may be uncertainty regarding the estimation of the optical efficiency and then a few degrees of the NOCT are fluctuated.

Moreover, the relationship between *NOCT* and $(T_{fi} - T_a)/I_T$ in the figure corresponds to that described in Eq. (13). The F_R value can be determined based on the slope of the plotted curve of Eq. (11) or (13). In addition, the F_R values at different mass flow rates are listed in Table 5; F_R and U_L increased with increasing mass flow. It could be noted that the value of $(\tau\alpha)$ was 0.67 which was similar to that of Sarhaddi et al. (2010).

With F_R, $(\tau\alpha)$, and U_L, the *NOCT* can be determined with Eq. (13). The NOCTs of the four investigated modules in series at a flow rate of 2.4 LPM are shown in Fig. 8. All curves exhibit similar relationships between *NOCT* and $(T_{fi} - T_a)/I_T$.

Fig. 9 shows the effect of the mass flow rate on the NOCT of the PVT module. The flow rates were varied from 1 to 6 LPM, and the NOCT decreased with increasing mass flow rate. However, when $(T_{fi} - T_a)/I_T$ exceeded 0.06, the NOCTs at any value of $(T_{fi} - T_a)/I_T$ were nearly identical for all flow rates. The correlation between the NOCT, $(T_{fi} - T_a)/I_T$, and mass flow rate, $\dot{m}$, of the tested module can be expressed as follows:

$$NOCT = 509.5\frac{T_{fi} - T_a}{I_T} - 0.7352\dot{m} + 36.94. \quad (14)$$

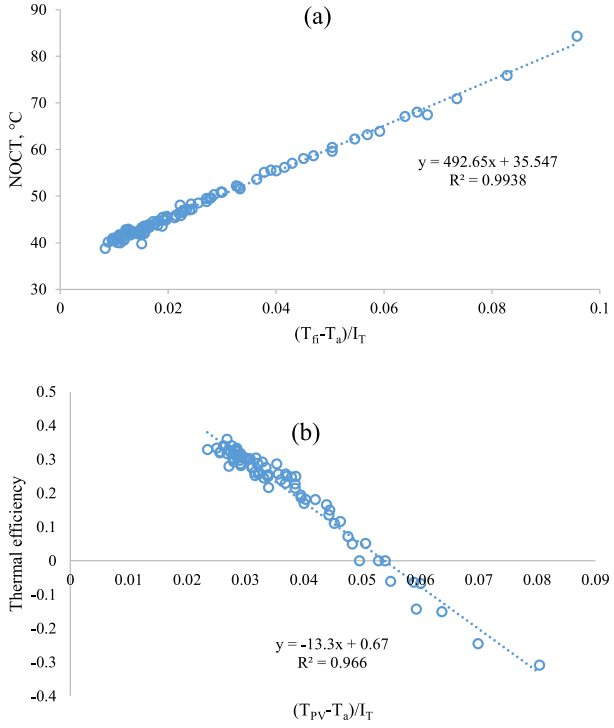

Fig. 7. Thermal performance of PVT at mass flow rate of 2.4 LPM: (a) NOCT, and (b) thermal efficiency.

The R^2 and RMSE values are 0.9795 and 1.223 °C, respectively.

4.3. Comparing current NOCT model with typical NOCT model

Fig. 10 shows the PVT module temperature at 2.4 LPM water circulation. The normal NOCT model was not affected by the fluid inlet temperature, and the module temperature decreased with the solar irradiance level; even the inlet temperature was high, particularly in the afternoon. Regarding the current NOCT model, the calculated results of the module temperature agree well with the experimental data.

Table 5
Thermal characteristics obtained in tests under no electrical load.

$\dot{m}$ LPM	$\dot{m}c_p$ J/Ks	A m^2	$800F_R$	$\frac{(\tau\alpha)}{U_L} \cdot (1 - F_R)\,800 + 20$	F_R	$(\tau\alpha)/U_L$	$(\tau\alpha)$	U_L
1	62.7	1.326	476.29	36.569	0.595	0.051	0.67	13.2
2.4	167.2	1.326	492.65	35.547	0.616	0.050	0.67	13.3
4	278.667	1.326	505.71	34.337	0.632	0.049	0.67	13.8
6	418	1.326	572.86	30.805	0.691	0.046	0.67	14.7

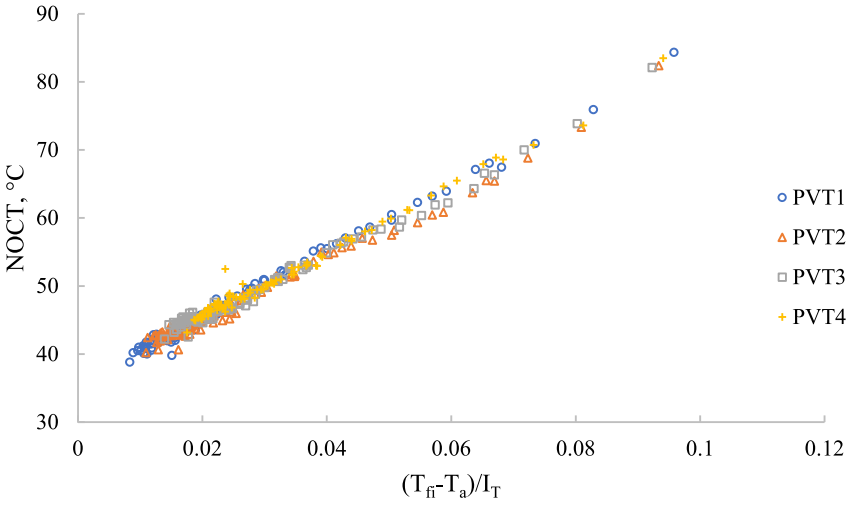

Fig. 8. NOCTs of four PVT modules in series obtained from experimental data at mass flow rate of 2.4 LPM in open-circuit mode.

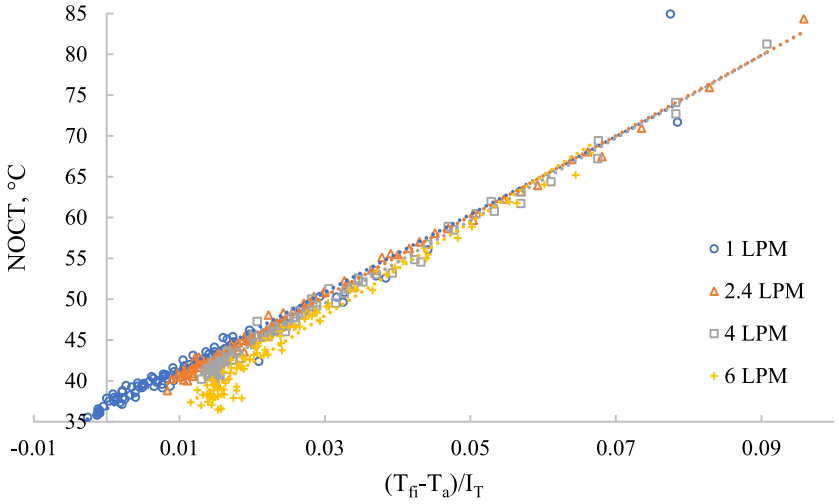

Fig. 9. Relationship between NOCT an $(T_{fi} - T_a)/I_T$ at different water mass flow rates.

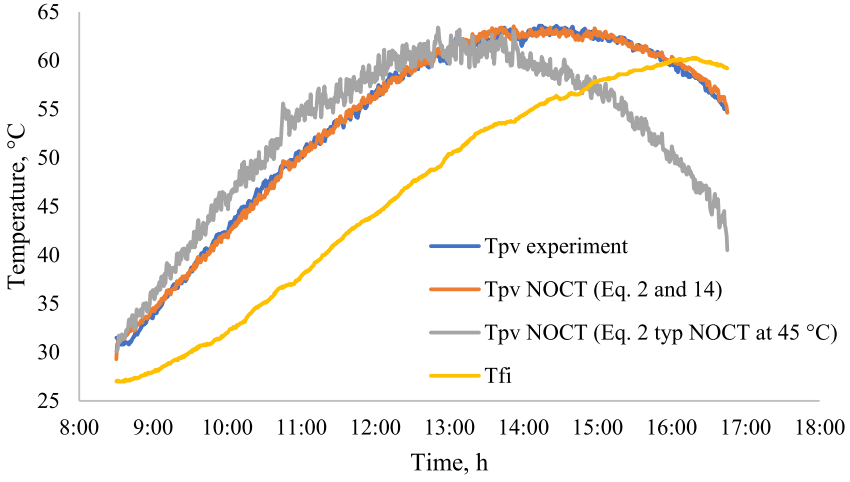

Fig. 10. Comparison of PVT module temperature of experiment ($T_{PV,exp}$) and calculation ($T_{PV,NOCT}$) based on Eqs. (2) and (14) and that of typical NOCT at 45 °C (February 10, 2019).

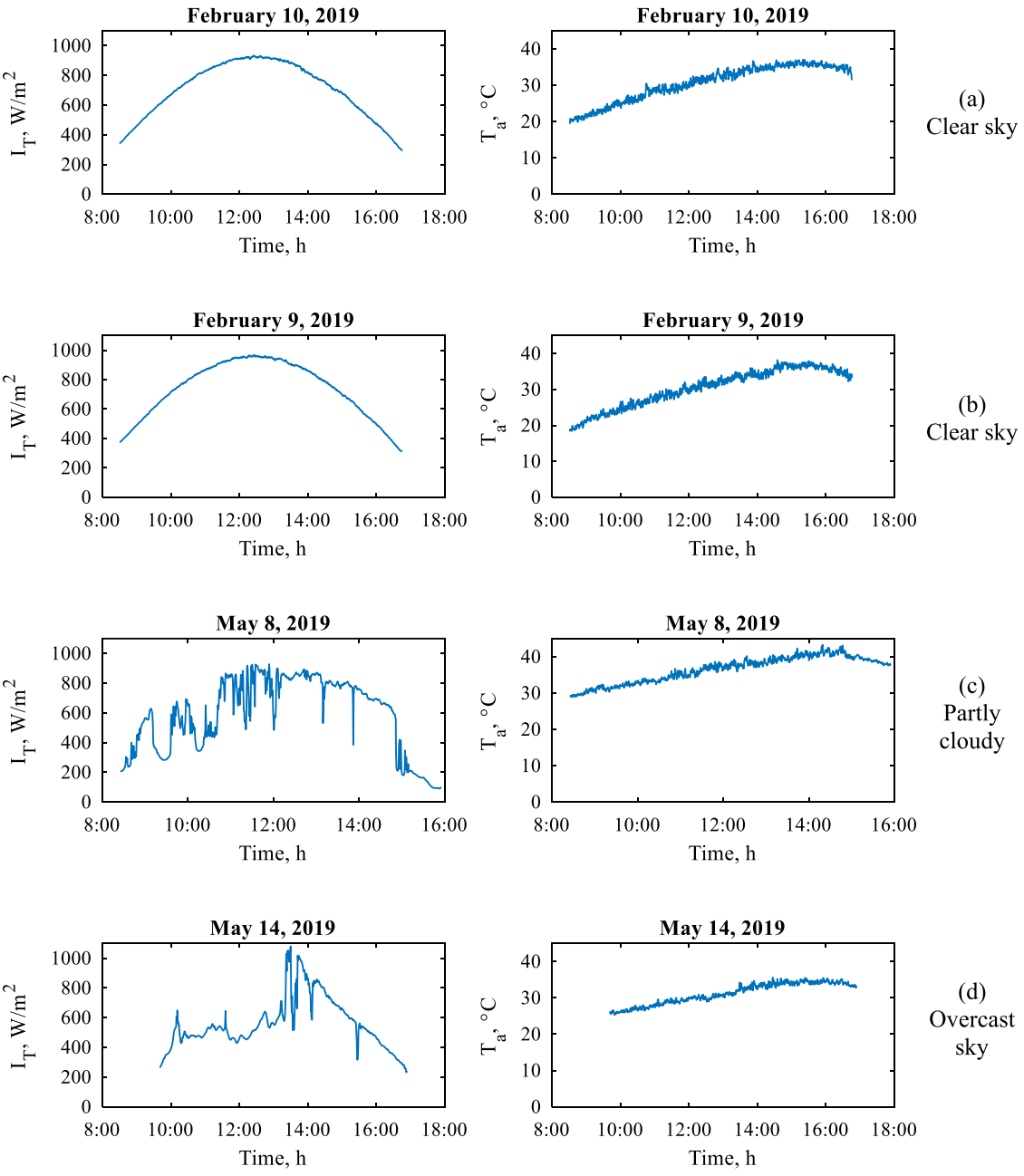

Fig. 11. Weather data of four days of experiments.

4.4. Validation of current NOCT model under various sky conditions

The developed NOCT model was used to predict the PVT module temperatures under no load, which was then compared with the experimental data of days with different sky conditions (Fig. 11). The results of all four PVT modules with water flow rates of 2.4 and 6 LPM are shown in Fig. 12. The RMSEs of all deviations were below 2 °C. Moreover, Fig. 13 shows the deviation of the predicted module temperatures with respect to the measured data; over 96% of the data exhibited deviations within ±10%.

4.5. Electrical performance

Fig. 14 compares the calculated maximum power point, P_m, based on Eq. (1) with the experimental data of the first PVT module (PVT1) recorded on clear-sky and overcast days. The calculated results of P_m agree well with the experimental data for all weather conditions with RMSE values of 2.8 and 5.1 W for the clear-sky and overcast-sky days, respectively; 94% of the calculated results agree well with the experimental data, with deviations of ±5%.

5. Conclusions

In this study, the performance of four PVT modules in series was investigated outdoors at various water mass flow rates and water inlet temperatures in the Chiang Mai climate. A new method for calculating the NOCT of PVT modules was developed, and the NOCT was used to evaluate the PVT module temperature and electrical power output. The conclusions are as follows:

- The NOCT of the PVT module depends on the incident solar irradiance, ambient temperature, fluid mass flow rate, and inlet temperature. Increase of the mass flow rate or decrease of the inlet temperature resulted in decrease of the NOCT.

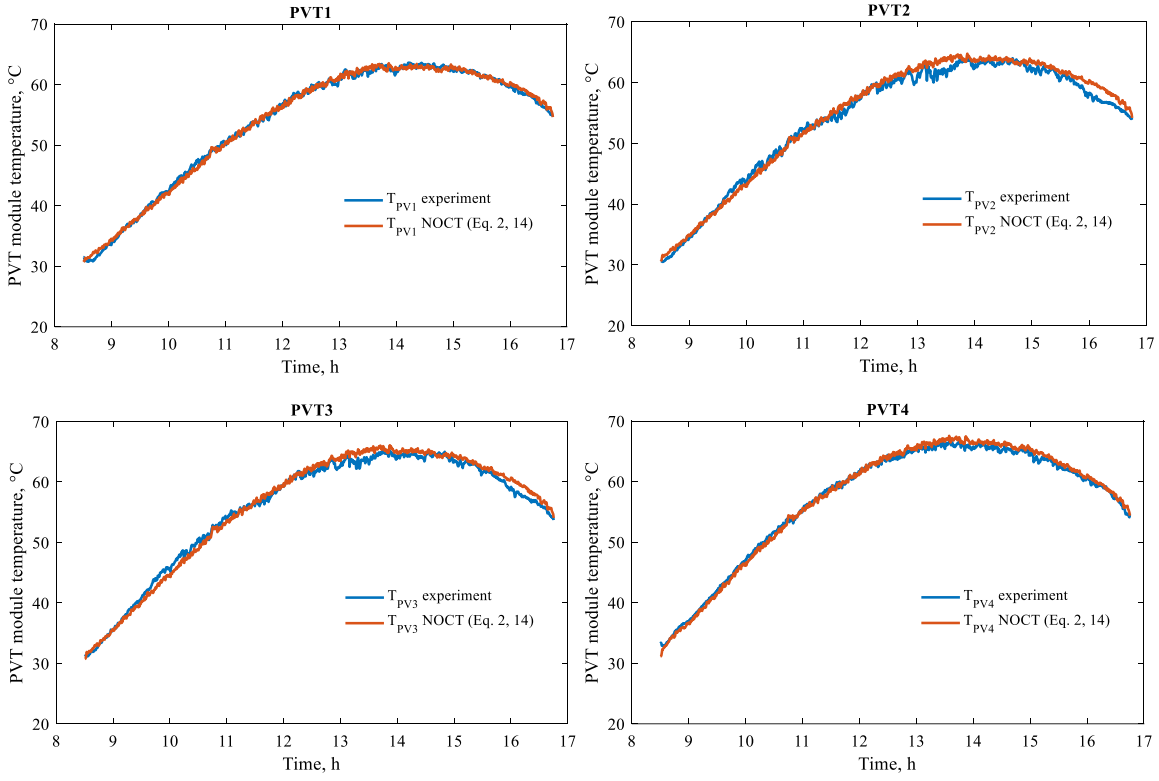

a. Clear-sky

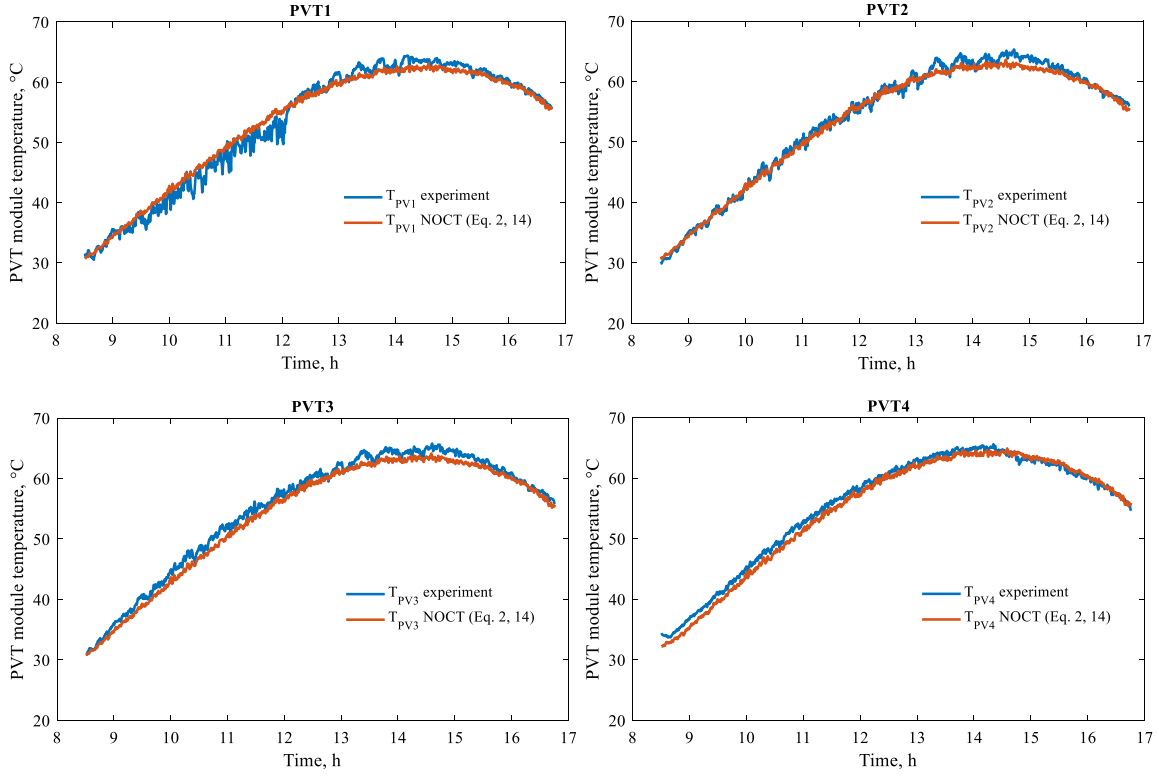

b. Clear-sky

Fig. 12. Validation of PVT module temperatures with experimental data: (a) clear-sky day with mass flow rate of 2.4 LPM, (b) clear-sky day with mass flow rate of 6 LPM, (c) partly cloudy day with mass flow rate of 2.4 LPM, and (d) overcast day with mass flow rate of 2.4 LPM.

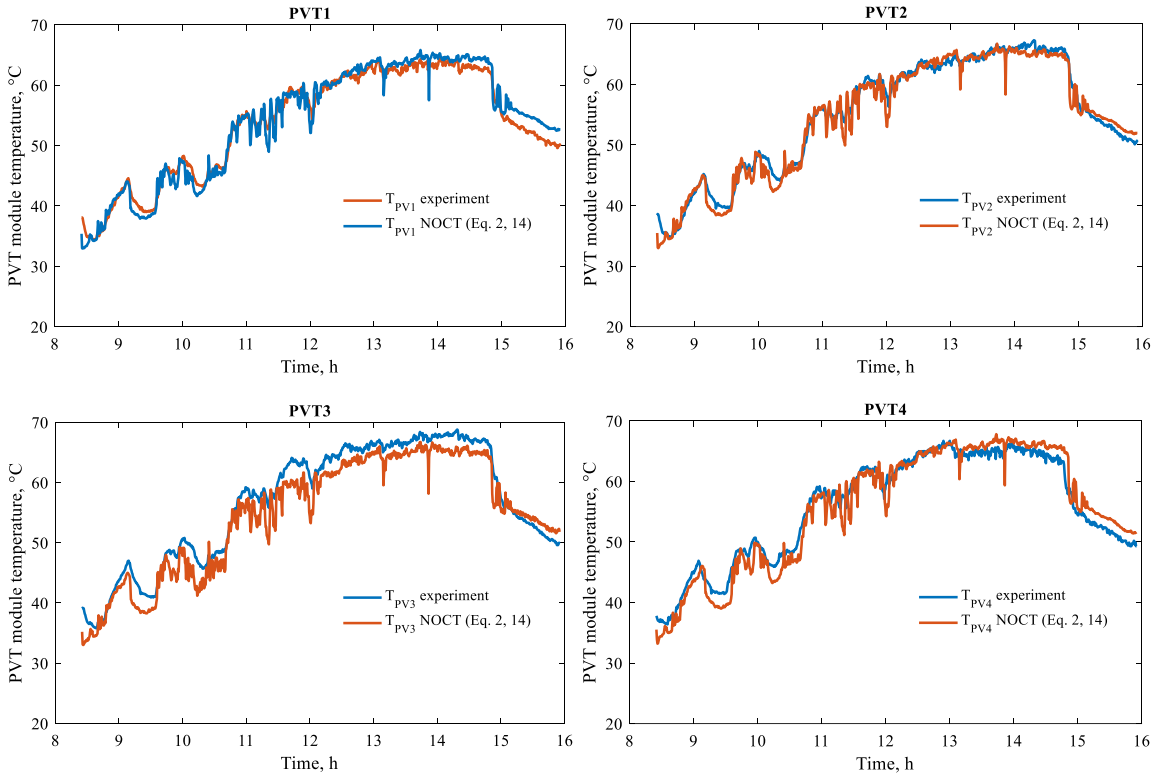

c. Partly cloudy

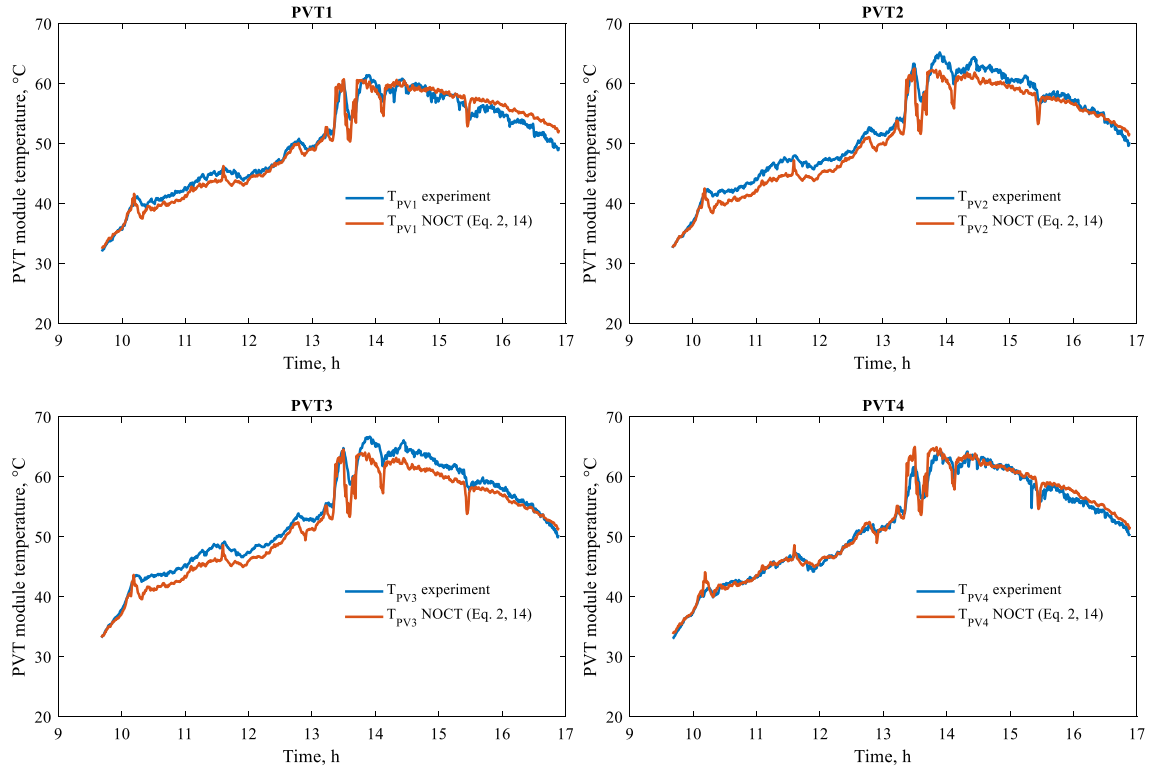

d. Overcast sky

Fig. 12. (*continued*).

- A new method for evaluating the NOCT of PVT modules was developed and presented, and the correlation between the NOCT of the tested unglazed PVT module, $(T_{fi} - T_a)/I_T$, and the mass flow rate was determined: $NOCT = 509.5\frac{T_{fi}-T_a}{I_T} - 0.7352\dot{m} + 36.94$. The corresponding calculated PVT module temperature agrees well with the experimental data for all

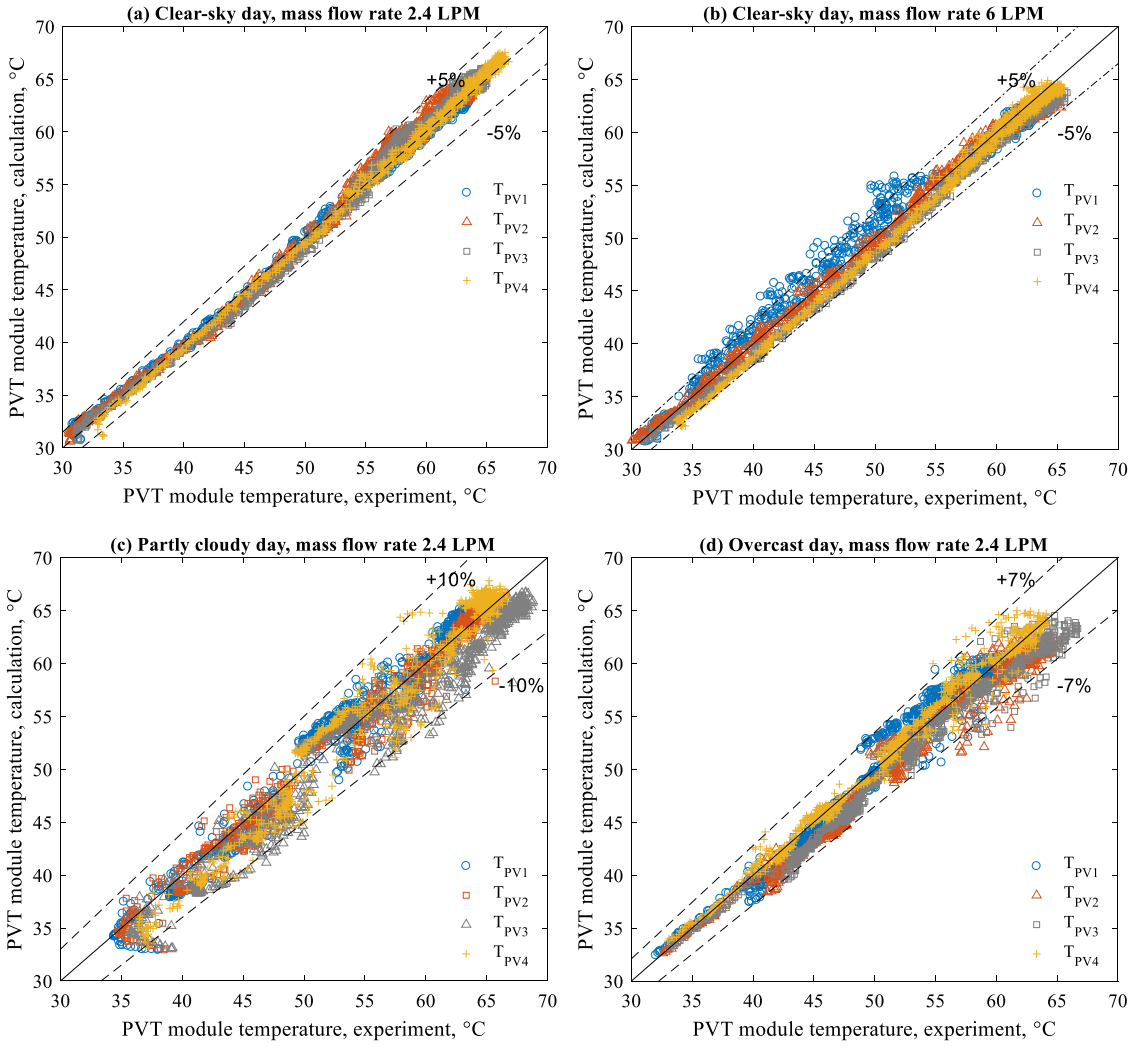

Fig. 13. Comparison of PVT module temperatures from calculations and experiments.

sky conditions. Over 96% of the calculated results has deviations within ±10% from the experimental data. In addition, the calculated electrical output of the PVT module agrees well with the experimental data, and 94% of the results has deviations within ±5% from the experimental data.

- The presented approach for evaluating the NOCT of PVT modules is practical: only F_R, $(\tau\alpha)$, and U_L of the PVT module are required, which can be determined in the same manner such as those of solar thermal collectors.

Declaration of competing interest

The authors declare that they have no known competing financial interests or personal relationships that could have appeared to influence the work reported in this paper.

Acknowledgments

This research project is supported by the Department of Mechanical Engineering Thailand, Faculty of Engineering Thailand, Chiang Mai University Thailand within the Research Assistant Program and the National Research Council of Thailand within the Project on Development of Alternative Energy Prototypes for Green Communities. In addition, this research study is partially supported by the Chiang Mai University Thailand.

Nomenclature

Abbreviation

LPM	Liter per minute
NOCT	Nominal operating cell temperature, °C
PVT	Photovoltaic thermal
$(T_{fi} - T_a)/I_T$	Reduced temperature, m^2 °C/W

Symbol

A	Area of solar cell module, m^2
c_p	Heat capacity, kJ/kg K
F_R	Module heat removal factor
I	Current, A
I_T	Solar irradiance, W/m^2
$\dot{m}$	Mass flow rate, kg/s
P_m	Maximum power point, W
$P_{m,stc}$	Maximum power point under the standard test conditions, W
$\dot{Q}_u$	Useful heat, W
$\dot{Q}_s$	Solar energy, W
T	Temperature, °C
T_a	Ambient temperature, °C
T_{fi}	Inlet temperature, °C
T_{fo}	Outlet temperature, °C

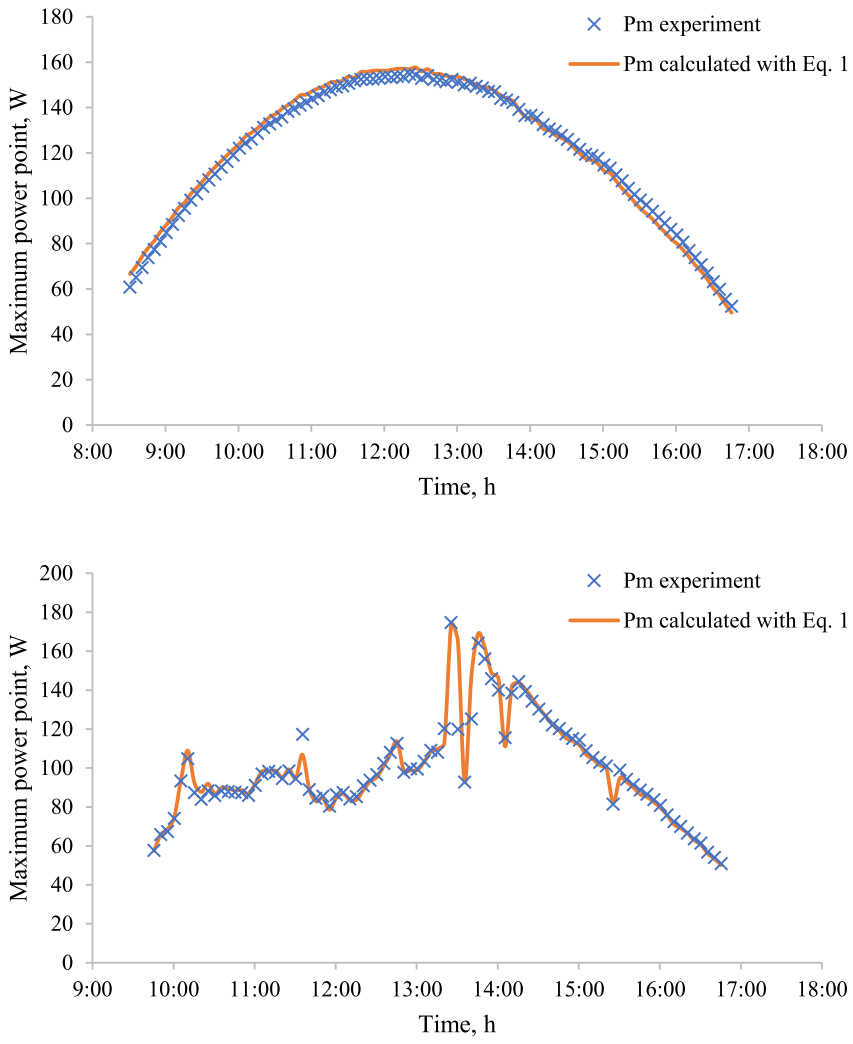

Fig. 14. Maximum power point of PVT1: (a) clear-sky day, February 10, 2019 and (b) overcast day, May 14, 2019.

T_{PV}	PVT module temperature, °C
U_L	Overall heat loss coefficient, W/m^2 K
V	Voltage, V
$(\tau\alpha)$	Optical efficiency of module
γ	Temperature coefficient of maximum power, 1/K
η_{th}	Thermal efficiency

Appendix

A.1. Uncertainty

The experimental uncertainty was calculated with the Gaussian prevalence law:

$$\omega_R = \sqrt{\left(\frac{\partial R}{\partial x_1}\omega_1\right)^2 + \left(\frac{\partial R}{\partial x_2}\omega_2\right)^2 + \cdots + \left(\frac{\partial R}{\partial x_n}\omega_n\right)^2},$$

where ω_R is the uncertainty of the output result and ω_1, ω_2, …, ω_n are the errors of the corresponding parameters.

A.2. Error analysis

The accuracy of the calculation results with respect to the experimental data can be calculated in terms of the root mean square error:

$$\text{RMSE} = \sqrt{\frac{\sum_{i=1}^{n}(y_i - x_i)^2}{n}},$$

where y_i is the calculated value, x_i is the experimental value, and n is the number of models or experimental data.

References

AL-Musawi, A.I.A., Taheri, A., Farzanehnia, A., Sardarabadi, M., Passandideh-Fard, M., 2019. Numerical study of the effects of nanofluids and phase-change materials in photovoltaic thermal (PVT) systems. J. Therm. Anal. Calorim. 137, 623–636. http://dx.doi.org/10.1007/s10973-018-7972-6.

Al-Shamani, A.N., Alghoul, M.A., Elbreki, A.M., Ammar, A.A., Abed, A.M., Sopian, K., 2018. Mathematical and experimental evaluation of thermal and electrical efficiency of PV/T collector using different water based nano-fluids. Energy 145, 770–792. http://dx.doi.org/10.1016/J.ENERGY.2017.11.156.

Al-Shamani, A.N., Sopian, K., Mat, S., Hasan, H.A., Abed, A.M., Ruslan, M.H., 2016. Experimental studies of rectangular tube absorber photovoltaic thermal collector with various types of nanofluids under the tropical climate conditions. Energy Convers. Manag. 124, 528–542. http://dx.doi.org/10.1016/j.enconman.2016.07.052.

Al Tarabsheh, A., Ghazal, A., Asad, M., Morci, Y., Etier, I., El Haj, A., et al., 2016. Performance of photovoltaic cells in photovoltaic thermal (PVT) modules. IET Renew. Power Gener. 10, 1017–1023. http://dx.doi.org/10.1049/iet-rpg.2016.0001.

Al-Waeli, A.H.A., Kazem, H.A., Chaichan, M.T., Sopian, K., 2019. Experimental investigation of using nano-PCM/nanofluid on a photovoltaic thermal system

(PVT): Technical and economic study. Therm. Sci. Eng. Prog. 11, 213–230. http://dx.doi.org/10.1016/J.TSEP.2019.04.002.
Anon, 2019a. Hybrid - solimpeks - volther powervolt n.d. http://www.solimpeks.com/volther-powervolt-en (accessed 16 April 2019).
Anon, 2019b. Li19 hand-held read-out unit / datalogger | hukseflux n.d. https://www.hukseflux.com/products/heat-flux-sensors/heat-flux-meters/li19-datalogger (accessed 16 April 2019).
Anon, 2019c. MS-602 pyranometer | EKO instruments n.d. https://eko-eu.com/products/solar-energy/pyranometers/ms-602-pyranometer (accessed 16 April 2019).
Atheaya, D., Tiwari, A., Tiwari, G.N., Al-Helal, I.M., 2016. Performance evaluation of inverted absorber photovoltaic thermal compound parabolic concentrator (PVT-CPC): Constant flow rate mode. Appl. Energy 167, 70–79. http://dx.doi.org/10.1016/J.APENERGY.2016.01.023.
Conti, P., Schito, E., Testi, D., 2019. Cost-benefit analysis of hybrid photovoltaic/thermal collectors in a nearly zero-energy building. Energies 12, 1582. http://dx.doi.org/10.3390/en12081582.
Duffie, J.A., Beckman, W.A., 2013. Solar Engineering of Thermal Processes. Wiley.
Fayaz, H., Rahim, N.A., Hasanuzzaman, M., Rivai, A., Nasrin, R., 2019. Numerical and outdoor real time experimental investigation of performance of PCM based PVT system. Sol. Energy 179, 135–150. http://dx.doi.org/10.1016/J.SOLENER.2018.12.057.
Fiorentini, M., Cooper, P., Ma, Z., 2015. Development and optimization of an innovative HVAC system with integrated PVT and PCM thermal storage for a net-zero energy retrofitted house. Energy Build. 94, 21–32. http://dx.doi.org/10.1016/J.ENBUILD.2015.02.018.
Florschuetz, L.W., 1979. Extension of the Hottel-Whillier model to the analysis of combined photovoltaic/thermal flat plate collectors. Sol. Energy 22, 361–366. http://dx.doi.org/10.1016/0038-092X(79)90190-7.
Fudholi, A., Sopian, K., Yazdi, M.H., Ruslan, M.H., Ibrahim, A., Kazem, H.A., 2014. Performance analysis of photovoltaic thermal (PVT) water collectors. Energy Convers. Manag. 78, 641–651. http://dx.doi.org/10.1016/j.enconman.2013.11.017.
Fuentes, M.K., 1987. A simplified thermal model for Flat-Plate photovoltaic arrays. Albuquerque, NM (USA).
Gaur, A., Ménézo, C., Giroux-Julien, S., 2017. Numerical studies on thermal and electrical performance of a fully wetted absorber PVT collector with PCM as a storage medium. Renew. Energy 109, 168–187. http://dx.doi.org/10.1016/j.renene.2017.01.062.
Guarracino, I., Freeman, J., Ramos, A., Kalogirou, S.A., Ekins-Daukes, N.J., Markides, C.N., 2019. Systematic testing of hybrid PV-thermal (PVT) solar collectors in steady-state and dynamic outdoor conditions. Appl. Energy 240, 1014–1030. http://dx.doi.org/10.1016/J.APENERGY.2018.12.049.
Guarracino, I., Mellor, A., Ekins-Daukes, N.J., Markides, C.N., 2016. Dynamic coupled thermal-and-electrical modelling of sheet-and-tube hybrid photovoltaic/thermal (PVT) collectors. Appl. Therm. Eng. 101, 778–795. http://dx.doi.org/10.1016/J.APPLTHERMALENG.2016.02.056.
Herrando, M., Pantaleo, A.M., Wang, K., C.N., Markides, 2019. Solar combined cooling heating and power systems based on hybrid PVT, PV or solar-thermal collectors for building applications. Renew. Energy 143, 637–647. http://dx.doi.org/10.1016/J.RENENE.2019.05.004.
Hossain, M.S., Pandey, A.K., Selvaraj, J., Rahim, N.A., Islam, M.M., Tyagi, V.V., 2019. Two side serpentine flow based photovoltaic-thermal-phase change materials (PVT-PCM) system: Energy, exergy and economic analysis. Renew. Energy 136, 1320–1336. http://dx.doi.org/10.1016/J.RENENE.2018.10.097.
Kazemian, A., Salari, A., Hakkaki-Fard, A., Ma, T., 2019. Numerical investigation and parametric analysis of a photovoltaic thermal system integrated with phase change material. Appl. Energy 238, 734–746. http://dx.doi.org/10.1016/J.APENERGY.2019.01.103.
Kern, E.C.J., Russell, M.C., 1978. Combined photovoltaic and thermal hybrid collector systems.
Lämmle, M., Oliva, A., Hermann, M., Kramer, K., Kramer, W., 2017. PVT collector technologies in solar thermal systems: A systematic assessment of electrical and thermal yields with the novel characteristic temperature approach. Sol. Energy 155, 867–879. http://dx.doi.org/10.1016/J.SOLENER.2017.07.015.
Liu, Z., Zhang, Y., Zhang, L., Luo, Y., Wu, Z., Wu, J., et al., 2018. Modeling and simulation of a photovoltaic thermal-compound thermoelectric ventilator system. Appl. Energy 228, 1887–1900. http://dx.doi.org/10.1016/J.APENERGY.2018.07.006.
Masters, G.M., 2004. Renewable and Efficient Electric Power Systems. John Wiley & Sons, Inc., Hoboken, NJ, USA, http://dx.doi.org/10.1002/0471668826.
Mattei, M., Notton, G., Cristofari, C., Muselli, M., Poggi, P., 2006. Calculation of the Polycrystalline PV Module Temperature using a Simple Method of Energy Balance, Vol. 31. http://dx.doi.org/10.1016/j.renene.2005.03.010.
Pantic, L.S., Pavlović, T.M., Milosavljević, D.D., Radonjic, I.S., Radovic, M.K., Sazhko, G., 2016. The assessment of different models to predict solar module temperature, output power and efficiency for Nis, Serbia. Energy 109, 38–48. http://dx.doi.org/10.1016/j.energy.2016.04.090.
Ramos, A., Chatzopoulou, M.A., Guarracino, I., Freeman, J., Markides, C.N., 2017. Hybrid photovoltaic-thermal solar systems for combined heating, cooling and power provision in the urban environment. Energy Convers. Manag. http://dx.doi.org/10.1016/j.enconman.2017.03.024.
Rejeb, O., Dhaou, H., Jemni, A., 2015. A numerical investigation of a photovoltaic thermal (PV/T) collector. Renew. Energy 77, 43–50. http://dx.doi.org/10.1016/j.renene.2014.12.012.
Ross, R.G.Jr., 1980. Flat-plate photovoltaic array design optimization. In: Photovolt Spec Conf 14th, San Diego, Calif, January (1980) 7-10, Conf Rec (A81-27076 11-44). Inst Electr Electron Eng Inc., New York, pp. 1126–1132, 1980, 1126–1132.
Sahota, L., Tiwari, G.N., 2017. Review on series connected photovoltaic thermal (PVT) systems: Analytical and experimental studies. Sol. Energy 150, 96–127. http://dx.doi.org/10.1016/j.solener.2017.04.023.
Sakellariou, E., Axaopoulos, P., 2018. An experimentally validated, transient model for sheet and tube PVT collector. Sol. Energy 174, 709–718. http://dx.doi.org/10.1016/J.SOLENER.2018.09.058.
Salem, M.R., Elsayed, M.M., Abd-Elaziz, A.A., Elshazly, K.M., 2019. Performance enhancement of the photovoltaic cells using Al2O3/PCM mixture and/or water cooling-techniques. Renew. Energy 138, 876–890. http://dx.doi.org/10.1016/J.RENENE.2019.02.032.
Sarhaddi, F., Farahat, S., Ajam, H., Behzadmehr, A., 2010. Exergetic performance assessment of a solar photovoltaic thermal (PV/T) air collector. Energy Build. 42, 2184–2199. http://dx.doi.org/10.1016/j.enbuild.2010.07.011.
Shyam, Tiwari, G.N., 2016. Analysis of series connected photovoltaic thermal air collectors partially covered by semitransparent photovoltaic module. Sol. Energy 137, 452–462. http://dx.doi.org/10.1016/J.SOLENER.2016.08.052.
Sun, V., Asanakham, A., Deethayat, T., Kiatsiriroat, T., 2018. Study on phase change material and its appropriate thickness for controlling solar cell module temperature. Int. J. Ambient Energy 1–10. http://dx.doi.org/10.1080/01430750.2018.1443500.
Teo, H.G., Lee, P.S., Hawlader, M.N.A., 2012. An active cooling system for photovoltaic modules. Appl. Energy 90, 309–315. http://dx.doi.org/10.1016/j.apenergy.2011.01.017.
Tiwari, G.N., Mishra, R.K., Solanki, S.C., 2011. Photovoltaic modules and their applications: A review on thermal modelling. Appl. Energy 88, 2287–2304. http://dx.doi.org/10.1016/J.APENERGY.2011.01.005.
Tripanagnostopoulos, Y., Souliotis, M., Battisti, R., Corrado, A., 2005. Energy, cost and LCA results of PV and hybrid PV/T solar systems. Prog. Photovoltaics Res. Appl. 13, 235–250. http://dx.doi.org/10.1002/pip.590.
Yu, Y., Long, E., Chen, X., Yang, H., 2019. Testing and modelling an unglazed photovoltaic thermal collector for application in Sichuan Basin. Appl. Energy 242, 931–941. http://dx.doi.org/10.1016/J.APENERGY.2019.03.114.